Wolbachia endosymbionts subvert the endoplasmic reticulum to acquire host membranes without triggering ER stress

Short title: endoplasmic reticulum subversion by *Wolbachia*

Authors

NourFattouh[1], Chantal Cazevieille[2] and Frédéric Landmann[1]

Affiliations

[1]CRBM, University of Montpellier, CNRS, France

[2]MRI-COMET, Plateau de microscopie électronique, U1051 INM

Hôpital Saint Eloi, Montpellier, France

Correspondence: frederic.landmann@crbm.cnrs.fr

Abstract

The reproductive parasite *Wolbachia* are the most common endosymbionts on earth, present in a plethora of arthropod species. They have been introduced into mosquitos to successfully prevent the spread of vector-borne diseases, yet the strategies of host cell subversion underlying their obligate intracellular lifestyle remain to be explored in depth in order to gain insights into the mechanisms of pathogen-blocking. Like some other intracellular bacteria, *Wolbachia* reside in a host-derived vacuole in order to replicate and escape the immune surveillance. Using here the pathogen-blocking *Wolbachia* strain from *Drosophila melanogaster*, introduced into two different *Drosophila* cell lines, we show that *Wolbachia* subvert the endoplasmic reticulum to acquire their vacuolar membrane and colonize the host cell at high density. *Wolbachia* redistribute the endoplasmic reticulum to increase contact sites, and time lapse experiments reveal tight coupled dynamics suggesting important signalling events or nutrient uptake. They however do not affect the tubular or cisternal morphologies. A fraction of endoplasmic reticulum becomes clustered, allowing the endosymbionts to reside in between the endoplasmic reticulum and the Golgi apparatus, possibly modulating the traffic between these two organelles. Gene expression analyses and immunostaining studies suggest that *Wolbachia* achieve persistent infections at very high titers without triggering endoplasmic reticulum stress or enhanced ERAD-driven proteolysis, suggesting that amino acid salvage is achieved through modulation of other signalling pathways.

Author summary

Wolbachia are a genus of intracellular bacteria living in symbiosis with millions of arthropod species. They have the ability to block the transmission of arboviruses when introduced into mosquito vectors, by interfering with the cellular resources exploited by these viruses. Despite the biomedical interest of this symbiosis, little is known about the mechanisms by which *Wolbachia* survive and replicate in the host cell. We show here that the membrane composing the *Wolbachia* vacuole is acquired from the endoplasmic reticulum, a central organelle required for protein and lipid synthesis, and from which originates a vesicular trafficking toward the Golgi apparatus and the secretory pathway. *Wolbachia* modify the distribution of this organelle to increase their interactions with this source of membrane and likely of nutrients as well. In contrast to some intracellular pathogenic bacteria, the effect of *Wolbachia* on the cell homeostasis does not induce a stress on the endoplasmic reticulum. One of the consequences of such a stress would be an increased proteolysis used to relieve the cell from an excess of misfolded proteins. Incidentally, this shows that *Wolbachia* do not acquire amino acids from the host cell through this strategy.

Introduction

The alpha-proteobacteria *Wolbachia* -*Wb*- are the most common endosymbionts encountered in nature, present in a plethora of terrestrial arthropod hosts, and in filarial nematode species. These reproductive parasites have developed a wide range of symbiotic interactions, from facultative to mutualistic [1]. In all

instances, they are vertically transmitted through the female germline but also colonize the soma [2]. The tissues that are infected can differ from one host species to another, as well as the *Wolbachia* intracellular titer. Although the highest titers are often observed in the germline, they vary considerably among wild isolates of specimens within a single species [3]. While *Wolbachia* intrinsic factors can be responsible for targeting specific cell types acting as reservoirs, i.e. the somatic stem cell niche in the *Drosophila* ovary [4], they can also influence the degree of intracellular replication. Such is the case for the pathogenic *Wolbachia* strain wMelpop, that possesses a region of eight genes called octomom, whose degree of amplification dictates the bacterial titer and the virulence [5]. Conversely, the host genetic background also exerts a profound influence on the bacterial ability to replicate. When the wMel strain naturally hosted in the fruit fly *Drosophila melanogaster* is transferred into the closely related *Drosophila simulans* species, mature oocytes appear dramatically more infected [6]. Therefore, depending on the permissivity of the genetic background, different cell types can harbor a wide range of endosymbiontic titers. As a consequence, the impact of a given *Wolbachia* strain on the cellular homeostasis, and the degree of subversion exerted on organelles to satisfy their obligate intracellular lifestyle can potentially induce variable phenotypes, i.e. in terms of nutrient demand, stress or cell innate immune responses.

These past years have seen a resurgence of interests in *Wolbachia* because they can be a drug target to fight parasitic filarial diseases [7], and because of their ability to compromise transmission of vector-borne arboviruses [8]. In the latter case, the wMel strain has been favored and introduced into mosquito vectors because it does not induce a fitness cost [9,10], allowing a spread through wild

100 populations of mosquitos. Although the mechanisms by which *Wolbachia* block
101 the pathogen transmission are not fully understood, a clearer picture starts to
102 emerge. However among recent studies, somewhat contradictory results have
103 been reported, reflecting a variety of phenotypes under environmental influence
104 (for a review see [11]). Typically, the role of *Wolbachia*-induced innate immunity
105 priming in pathogen interference is still an object of debate, although viral
106 replication inhibition can be achieved by wMel without inducing an upregulated
107 expression of anti-microbial peptide genes [12,13]. *Wolbachia* depend on host
108 nutrients such as amino acids and lipids [14,15], but they potentially provision
109 their hosts to act in some instances as nutritional symbionts. Hence, the cost and
110 benefit associated with a *Wolbachia* infection are certainly variable. Nonetheless
111 their intracellular lifestyle involves a competition with viruses for subverting the
112 same limited resources. Cholesterol and lipid homeostasis are modulated in the
113 presence of *Wolbachia* [16] and account for their pathogen-blocking effect,
114 limiting the viral access to these metabolites essential to their replication
115 [17,18]. If a persistent infection with *Wolbachia* endosymbionts exerts a cellular
116 stress, it should not affect the host viability. An Endoplasmic Reticulum -ER-
117 stress response has been described to be associated with *Wolbachia* [18,19]. The
118 ER is involved in lipid metabolism, protein synthesis and their proper folding as
119 well as post-translational modifications, and is the source of vesicular trafficking
120 with the Golgi apparatus [20]. Because of its central role in the host cell
121 metabolism, the ER is often subverted by viruses and intracellular bacteria
122 [21,22]. When the cell homeostasis is perturbed to the point that misfolded
123 proteins accumulate in the ER, an Unfolded Protein Response -UPR- is triggered.
124 In order to restore homeostasis, the ER protein folding capacity is increased

125 through chaperone release in the ER lumen and upregulation of chaperone and
126 UPR sensor genes; translation is reduced; and an ER-associated degradation
127 ERAD- pathway is upregulated. If the stress is prolonged, cell dysfunctions occur
128 and cell death is eventually induced [23]. Accordingly, some intracellular
129 bacteria have learned to subvert and control the UPR to avoid such fate [22]. It is
130 therefore intriguing that an ER stress has been reported or suggested by some
131 studies and up to date invoked as a consequence of a *Wolbachia* infection. More
132 specifically, proteomic studies suggest a mild upregulation of some UPR related
133 genes, although it should be noted that they were carried out with the life-
134 shortening pathogenic strain wMelpop [18]. A recent study using RNAi
135 screening in *Drosophila* cells coupled to electron microscopy observations,
136 highlights the requirement of an ERAD ubiquitin ligase to maintain a normal
137 *Wolbachia* titer, and reports a close subcellular vicinity between *Wolbachia* and a
138 morphologically aberrant ER [19]. This study suggests that an ERAD-derived
139 proteolysis is induced by *Wolbachia* to salvage amino acids. In the present study,
140 we seek to clarify the link between *Wolbachia* and the ER by exploring the
141 physical relationship between the endosymbiont intracellular population and
142 this organelle at the cellular level as well as the functional consequences of a
143 *Wolbachia* infection on the ER. To avoid cell line-specific phenotypes and to take
144 in account the impact of the host genetic background, two cell lines showing
145 different gene expression profiles have been infected with the same wMel strain.
146 Specifically, live studies and observation of fixed cells reveal a complex and
147 dynamic interaction between wMel and the ER. This organelle, and not the Golgi
148 apparatus as previously suggested, appears to be the source of the endosymbiont
149 vacuolar membrane. *Wolbachia* redistribute the ER without triggering

pathological morphologies. In addition, gene expression analyses indicate that UPR and ERAD key players are not upregulated upon *Wolbachia* infection, and immunostaining studies of ubiquitin chains with degradative roles confirm that ERAD-derived proteasomal degradation is not increased, suggesting that *Wolbachia* do not induce ER stress and proceed through subversion of other host pathways to salvage amino acids.

Results

The host genetic background influences the *Wolbachia* titer in *Drosophila* cell cultures.

In order to gain insights into the general mechanisms of host cell subversion operated by the *Wolbachia* strain wMel in its natural host *D. melanogaster* to sustain its intracellular lifestyle, and to minimize cell line-specific phenotypes, we established new wMel infections in two *D. melanogaster* cell lines described to display distinct gene expression profiles [24]. The two selected cell lines are adherent, facilitating cellular analyses on live and fixed samples. While both cell lines express about 6,000 genes, nearly half of them show considerable expression variations between cell lines. 1182-4H is an acentriolar haploid cell line derived from maternal haploid *mh 1182* mutant embryos [25,26]. S2R+ are tetraploid male cells derived from the original Schneider's cell line [27,28]. We chose to introduce in these two different genetic backgrounds a wMel strain derived from JW18, very closely related to the wMel genome of reference [28]. The infected JW18 cell line has been commonly used in numerous studies as a

reference cell line to explore the *Wb*-host interactions and the *Wb*- induced viral protection at the cellular and molecular levels [19,28–31]. To infect naive cell lines, wMel bacteria were purified from JW18 cell cultures and added to flasks of uninfected 1182-4 and S2R+ cells (See Methods). JW18 cells harbor fluorescent GFP-Jupiter decorated microtubules. This helped us to confirm the exclusion of cell contaminant during the infection process. After one month, we found the infection to be partial in both cell lines, and an infection dynamics time course experiment confirmed the slow progress of the infection (S1A Fig). Another round of infection was then repeated, leading to stably infected cell lines as determined by immunofluorescence with an anti-*Wolbachia* surface protein - WSP- antibody (See Methods and Fig 1A to C'), named hereafter 1182-4 *Wb* and S2R+ *Wb*. The vast majority of cells is infected in 1182-4 *Wb*, and the infection is total in S2R+ *Wb*. The *Wb* titer is also much higher in S2R+ *Wb* compared to 1182-4 *Wb,* reaching several hundreds of endosymbionts per individual cells (Fig 1B',C'; S1 and S2 movies). These high *Wb* titers do not significantly affect the host cell viability (Sup1B Fig). We used the WSP-associated fluorescence area, expressed as a percentage of the total cell surface, acquired from full confocal image projections as a proxy to quantify the *Wb* titer in both cell lines (Fig 1D). We concluded that the S2R+ genetic background is more permissive to the wMel infection.

The Golgi apparatus distribution and morphology are not affected by the presence of *Wolbachia*.

Using a moderate and variable *Wb* titer in 1182-4 *Wb* on one hand, and a remarkably high *Wb* titer in S2R+ *Wb* on the other hand, we sought to describe

the influence of the *Wb* endosymbionts on the host cell physiology, taking into account the *Wb* level. The subcellular distribution of organelles is tightly linked to their function [32], and can be affected together with their morphology, by intracellular pathogens [33]. The *Wb* reside into a vacuole made of a host-derived membrane. Previously *Wb* and the Golgi cisternae were described to reside in the same subcellular compartment close to centrioles in the *Drosophila* embryo, therefore the Golgi apparatus has been proposed to be the source of the *Wb*-containing vacuole [34]. Moreover the Golgi apparatus can be subverted and fragmented by intracellular pathogens such as *Chlamydia*, that are surrounded by Golgi ministacks to facilitate lipid acquisition [35]. We reasoned that the amount, the localization and the morphology of the organelle providing membranes to the *Wb*-containing vacuoles may be potentially affected in a *Wb* titer-dependent manner. To investigate the relationship between *Wb* and the Golgi apparatus, S2R+ and acentriolar 1182-4 cells were both co-stained with an anti- *Wb* surface protein - anti-WSP- and a cis-Golgi marker -GM130-, in presence and absence of endosymbionts (Fig 2A). The Golgi apparatus typically displays cell type-specific patterns, and the cis-Golgi often appears as large foci in 1182-4 cells, and as many smaller foci in S2R+ cells. When the *Wb* do not fill the entire cytoplasm, i.e. in 1182-4 *Wb* cells, a thorough visual inspection did not allow us to draw a correlation of subcellular localization between the endosymbionts and the Golgi apparatus. In addition, the number and size of GM130-positive foci did not appear influenced by the abundance of *Wb* endosymbionts in either infected cell lines (i.e. Fig 2A dashed lines for cells with either high or low *Wb* levels, and B). Unlike in a previous report establishing the Golgi apparatus as a source of vacuolar membrane, we never observed GM130-positive *Wb* vacuoles [34]. We

next checked the morphology of the Golgi apparatus in presence of *Wb* by ultrastructural studies (Fig 2C). The Golgi cisternae appeared properly arranged, and we could not detect any morphologies that would differ from non-infected cells, despite heavy loads of endosymbionts in the S2R+ *Wb* cell line. Together, this data set suggests that the Golgi apparatus does not appear to be subverted by *Wolbachia* at the subcellular level, and does not support the hypothesis of this organelle being a source of membrane for the endosymbionts.

Wolbachia interact with the Endoplasmic Reticulum, source of their vacuolar membranes.

A previous study based on electronic microscopy has reported observations of *Wb* in close contact with ER tubules, and in some instances a continuum between the ER and the *Wb* vacuolar membrane [19]. To better understand how and to what extent the *Wb* intracellular population interact globally with the ER, we performed simultaneous live observations of the endosymbionts and of this organelle. To this end, we used the SYTO 11 DNA live dye that stains preferentially *Wb* [36], and an ER tracker, that recognizes the sulfonylurea receptors of ATP-sensitive K+ channels located on ER membranes. We first performed confocal time lapse fluorescence imaging of 1182-4 *Wb* cells. Cortical areas enriched in tubular ER were chosen for time lapse analyses because they offer a better resolution of these dynamic structures (Fig 3A). We typically observed three categories of *Wb*. Some peripheral *Wb* clusters did not show any obvious interactions with the ER (Fig 3A grey arrows), some were juxtaposed to the ER and displayed tightly coupled dynamics (Fig 3A orange arrow), while few *Wb* appeared to be localized within dynamic ER tubules (Fig 3A yellow

arrowhead, and see S3 movie that recapitulates these observations). We next used the same fluorescent markers in 1182-4 *Wb* and S2R+ *Wb* cells to score the different types of interaction between *Wb* and the ER (Fig 3B). Striking differences appeared in these two different cellular environments. While in random focal planes 62% of *Wb* did not reside in close ER vicinity in 1182-4 *Wb* cells, only 2% were distant from the ER in S2R+ *Wb* cells. Hence a majority -80%- of endosymbionts were in close contact with the ER in S2R+ *Wb*, while only 34% contacted the ER in the 1182-4 genetic background. Interestingly 17% in S2R+ *Wb* and 9% in 1182-4 *Wb* appeared either inside the ER and/or surrounded by an ER tracker-positive membrane (Fig 3C). Together this dataset shows that the physical interaction of *Wolbachia* with the ER is highly dynamic. The presence of ER tracker around some endosymbionts strongly suggests that this organelle is a source of vacuolar membrane. Some *Wb* were detected in ER tubules, and only a minority of endosymbionts display an ER tracker-positive vacuolar membrane, leading us to hypothesize that they may represent newly acquired membranes, whose composition is subsequently modified by *Wb* (i.e. less or no ATP-sensitive K+ channels leading to ER tracker-negative *Wb* vacuoles). In addition, time lapse recordings showing *Wb*-ER coupled dynamics reveal a tight physical interaction between the *Wb* vacuole and this organelle, suggesting potential signaling events and/or possible nutrient uptake. The increased association of *Wb* with the ER in a S2R+ genetic background, highly permissive to the *Wb* infection, suggests that the ability to subvert the ER is crucial for *Wolbachia* to thrive intracellularly.

The ER subcellular distribution is affected by *Wolbachia.*

Because the ER-*Wb* contacts are prominent in S2R+, we first examined the ER by confocal microscopy to assess the impact of *Wb* on its distribution. In non-infected cells, the ER appears principally composed of a dense perinuclear network of tubules and vesicles, while cisternae are less detectable. The cell periphery and cortical areas are enriched with ER tubules, which are often branched (Fig 4A). In contrast, in infected cells a fraction of the ER becomes heavily clustered close to the nucleus (Fig 4A cyan arrows), while cytoplasmic regions harboring *Wb* are highly enriched in tubular ER (Fig 4A yellow arrowheads and bottom row).

We defined this mass of ER as "ER clusters", which is greatly enhanced by the presence of *Wb* in both cell lines (Fig 4B). We wondered whether this ER distribution was a consequence of an ER stress, and S2R+ were treated with tunicamycin, an ER stress inducer, which did not increase the occurrence of this phenotype compared to untreated S2R+ cells (Fig 4B). ER morphological aberrations that may not be detectable by confocal fluorescence microscopy have been reported in *Wb*-infected cells such as ER tubule swelling and an increase in cisternae [19], leading us to perform EM ultrastructural studies on s2R+ *Wb* and 1182-4 *Wb* cells, and on their naive counterparts (Fig 4C,D). The dark ER mass is easily distinguishable in infected cells -thick red arrows-. A closer look at this cluster reveals it is composed of randomly - thin green arrows- and orderly -thin red arrow- packed tubules or cisternae. No swollen structure was detected within these clusters in either cell types. In the periphery, multiple *Wb* share very often a same vacuole, tightly apposed to rough ER -cyan arrows, and bottom image-. Incidentally, these multi-*Wb* vacuoles were encountered much more frequently in the highly permissive S2R+ genetic background

compared to 1182-4. We then searched for a size increase of cisternae and swollen ER tubules without success in S2R+ *Wb.* Measurements of ER inter membrane distances by electron microscopy however revealed very marginal ER swelling in 1182-4 *Wb*, not affecting the average thickness of ER in this cell line (Fig 4D). Last, because of the dramatic ER redistribution observed in S2R+ *Wb* occurring in more than half of these infected cells, we investigated at the individual cell level the impact of this ER defect on the Golgi apparatus distribution (Fig 4E). In non-infected cells, the Golgi foci are surrounded throughout the cell periphery by large amounts of the ER (Fig 4E left upper and lower panels, yellow arrowheads point to Golgi foci). In *Wb*-infecting cells showing ER clusters, the Golgi units do not coalesce toward the ER mass (Fig 4E right panel top images), and their distribution is not appear significantly perturbed. Although they remain associated with some ER (Fig 4E yellow arrowheads on bottom images), the overall distance between most of the ER and the Golgi apparatus is increased. In conclusion, *Wolbachia* dramatically redistribute the ER without affecting its luminal width, since we did not observe any ultrastructural variations in presence of the endosymbionts. The high titer in S2R+ *Wb* correlates with a tight association of *Wb* with the ER, and in general a large fraction of this organelle becomes spatially restricted, close to the nucleus, upon a *Wb* infection. This defect could potentially affect its function and interactions with other organelles such as the Golgi apparatus. Attempts to phenocopy the ER compaction with tunicamycin did not succeed, suggesting that this redistribution is operated by *Wb* independently of a potential ER stress.

Wolbachia do not induce ER stress in 1182-4 and S2R+ genetic backgrounds

We next sought to examine the impact of a *Wb* infection on the ER functions. To ensure protein homeostasis in the cell, one of the role of the ER is to control the proper folding and maturation of proteins through the unfolded protein response -UPR-, upregulated when misfolded proteins accumulate. When these adaptive responses are not sufficient, the endoplasmic-reticulum-associated protein degradation -ERAD- pathway is in turn activated to target and retrotranslocate ER misfolded proteins to the cytosol, where they are addressed towards a degradation pathway by the ubiquitin-proteasome machinery [37]. We first checked whether the ERAD function was subverted in order to provision *Wb* with amino acids derived from an increased proteolytic activity, as previously suggested in *Wb*-infected JW18 cells [19]. We first stained cells with the FK2 antibody recognizing all mono- and polyubiquitylated proteins, but not the free ubiquitin, considered as a good proxy to assess proteasomal degradation-associated polyubiquitylation marks - K48 and K11 poly-Ub - , since these degradation marks are the most abundant among polyubiquitylated chains in the cell [38] (See Methods and Fig 5A). We quantified the total fluorescence surface associated with the polyubiquitylation foci on full confocal projections, and we found the presence of *Wb* to correlate with 2.5 and 4.2 times as many polyubiquitylation in 1182-4 and S2R+ genetic backgrounds respectively (Fig 5A,B). We reasoned that a proteasomal degradation-linked poly-Ub signal, reflecting a *Wb*-dependent amino acid demand, should vary according to the endosymbiont titer, that is variable between cells in a given infected cell line. We chose the 1182-4 *Wb* cell line showing fewer heavily infected cells to perform a

linear regression highlighting the amount of FK2 foci in function of an increasing *Wb* titer (Fig 5C). We found no correlation between the *Wb* titer and the number of FK2 foci. This suggests that the observed FK2 signal is unlikely to account for an increased proteasomal degradation. To verify this result, we next checked specifically the levels of K11 poly-Ub chains by immunostaining analyses. K11 is the ubiquitin linkage primarily generated by the ERAD pathway [39]. We failed to detect any differences between infected and non-infected cells (Fig 5D). In the fraction of S2R+ *Wb* cells endowed with high *Wb* levels, the ER becomes clustered in an area from which the endosymbionts are excluded. Focusing our attention on these areas to detect a possible enrichment of ER-associated K11 poly-Ub, we did not detect an increase of this ERAD-associated degradation mark (Fig 5D, dashed yellow circle). Both K11- and K48- linked poly-Ub chains are involved in ERAD [40], therefore we checked the levels of K48 poly-Ub, that also appeared undistinguishable in infected cells compared to their non-infected counterparts (S2 Fig.). Together these results indicate that the global increase of cellular polyubiquitylation in presence of *Wolbachia* does not reflect an increase in proteasomal degradation- associated K11/K48 polyubiquitylation marks.

We decided to perform quantitative PCR analyses to investigate the UPR and ERAD responses at the gene expression level in the presence of *Wb*, in order to characterize the level of ER stress potentially generated by the endosymbionts. Briefly, upon a stress leading to accumulation of misfolded proteins, the ER transmembrane stress sensors PERK, ATF6, and IRE1 release the chaperone Bip in the ER lumen, and an UPR response is activated. This response aims at decreasing protein translation and enhancing the protein folding capacity in the ER, by upregulating the expression of chaperones and UPR sensors (Fig 6A and

374 [41]), while the ERAD pathway drives misfolded protein to undergo proteolysis.
375 We first selected *D. melanogaster* genes confirmed to respond to tunicamycin-
376 induced ER stress, and that are involved in both UPR and ERAD responses [42].
377 We next monitored these candidate genes in the 1182-4 genetic background by
378 submitting the cell line to a tunicamycin treatment for 48 hours at 10 µg/mL (Fig
379 6B). We found a ~2 fold gene expression upregulation for the three UPR sensors
380 *perk/gcn2*, *atf6* and *ire1* (Fig 6A, B top graphs). In addition, a number of ERAD
381 key players, the *derlin* orthologs *der-1* and *der-2, sel1L/hrd3 and hrd1/sip3*
382 whose products associate to form a complex, as well as members of the ubiquitin
383 ligase complex were upregulated from 3 to more than 5 folds. With this
384 experiment validating the 1182-4 cell line responsiveness to ER stress, we next
385 measured the impact of *Wb* on this stress in the 1182-4 *Wb* (Fig 6B bottom
386 graphs). We did not detect any induction of the UPR sensors or downstream
387 targets. Similarly, none of the ERAD key players that responded to tunicamycin
388 were affected by the presence of *Wb*. This shows that *Wolbachia* do not trigger
389 an ER stress response leading to increased UPR and ERAD activities in 1182-4
390 *Wb* cells. Last, we verified the level of ER stress in S2R+ *Wb* cells using a
391 fluorescent ATF-4 activity reporter gene -the translational inhibitor 4E-BP- that
392 responds to the PERK/GCN2- ATF4 pathway through ATF4 binding sites [43].
393 The fluorescence was monitored 48 hours after transfection with the 4E-BP
394 intron dsRed reporter, and a tunicamycin treatment was added as a positive
395 control of ER stress (Fig 6C, and Methods). Transfected cells showed in presence
396 of tunicamycin high nuclear and cytoplasmic fluorescence levels. Quantification
397 of the fluorescence revealed a level of ATF4 signaling activity upon ER stress 4
398 times higher on average compared to non-treated S2R+ cells. The fluorescence

399 levels expressed in S2R+ *Wb* cells appeared similar to what observed in S2R+
400 cells, suggesting that the presence of *Wb* do not cause a significant stress in the
401 S2R+ genetic background. Altogether, this data set suggests that in these two
402 host cell genetic backgrounds, the *Wolbachia* can proliferate and persist in a
403 stable manner without triggering ER stress and in particular the ERAD pathway,
404 implying that other mechanisms than ERAD-induced proteolysis should exist to
405 salvage amino acids.
406

407 Discussion

408

409 A number of studies these past years have started to investigate the basis
410 of the *Wb* intracellular lifestyle and their impact on the cell homeostasis using *in*
411 *vitro* cell culture models (i.e. [13,16,18,19,44,45]). The results of these studies
412 can be variable depending on the *Wb* strain and the infected insect cell lines. In
413 order to minimize the bias of a cellular context potentially leading to cell line-
414 specific phenotypes, we infected two genetic backgrounds presenting an
415 important variation at the level of the expressed genes [24]. Additionally, the two
416 cell lines were infected with a single wMel strain, that derives naturally from *D.*
417 *melanogaster.*

418 Here we identified the endoplasmic reticulum as a source of vacuolar
419 membranes for *Wolbachia* in *D. melanogaster* species, and we observed close
420 appositions between the replicative vacuole of these endosymbionts and the ER
421 membrane. These appositions are likely to lead to the biogenesis of ER-derived
422 *Wb* vacuoles, while sometimes allowing fusion with this organelle. Coupled
423 dynamics between *Wb* and the ER tubules seen in time lapse microscopy reveals

tight and prolonged interactions, supporting as well the possibility of nutrient uptake from the ER. The cellular context greatly influences the *Wb* titer, and a permissive environment correlates with more apposition events with the ER, suggesting that the ability of *Wb* to subvert the ER in a given environment correlates with growth and replication. A *Wb* infection redistributes the ER, and while a tubular network associates with the endosymbionts, a significant fraction of this organelle shrinks to become compacted close the cell nucleus. Although the functional impact of this ER clustering remains unclear, the ultrastructural ER organization does not reveal swollen compartments or more cisternae. Gene expression analyses of central ER stress players, as well as immunofluorescent studies of ERAD-induced proteolysis key marks indicate that the *Wb*-induced ER subversion does not trigger the UPR nor an increased proteolysis. Hence the *Wb* level, whether low or high, does not seem to perturb the ER-regulated mechanisms of cell homeostasis in a significant manner. Incidentally, these results indicate that *Wb* is likely to rely on other sources than ERAD-induced proteolysis to salvage amino acids.

The *Wolbachia* endosymbionts are transmitted vertically in their arthropod or filarial nematode hosts, from mothers to their offspring. Once in the egg they next colonize specific somatic tissues and the germline during embryonic and larval developmental stages, following asymmetric segregation during cell mitotic divisions [2]. Although a germline tropism has been described, implying that *Wb* can pass from cell to cell either artificially in *Drosophila* through abdominal injections of purified *Wb*, or through a developmentally regulated colonization of the filarial nematode ovary [46,47], they do not share with most intracellular pathogens the ability to easily infect

449 naïve cells, thus limiting their horizontal transfers. It has been demonstrated that
450 *Wb* can pass from infected to non-infected cell in *in vitro* assays, without
451 requiring cell-to-cell contact, possibly through secretion [30]. If active
452 mechanisms of cell entry are not precisely described, passive uptake
453 mechanisms through phagocytosis explain at least in part their entry in cell
454 culture assays. To optimize the infection of naive cell lines, we set up a protocol
455 of *Wb* enrichment from a *Wb*-infected cell culture. This allowed us to expose cells
456 to very high bacterial concentrations. Although *D. melanogaster* cell cultures
457 have a strong capacity of engulfment –which does not make them an ideal model
458 to study mechanisms of bacterial cell entry-, artificial infections of naïve cell
459 culture with *Wolbachia* remain nonetheless a slow process. The fact that a
460 significant proportion of cells remained uninfected after one month suggests
461 indeed that extracellular *Wb* originating from possible secretion or dead cells do
462 not have strong infection capacities and that colonization of a naïve environment
463 remains a challenge. This is in part due to their slow replication cycle estimated
464 to last 14 hours [48], but it is also very likely that some *Wb* do not succeed in
465 escaping autophagy. Those nonetheless succeeding at surviving and replicating
466 not only need to modify the phagosome membrane along the endocytic pathway
467 to avoid the cell surveillance, but also need to acquire new membranes and
468 nutrients.

469 The ER represents a nutrient-rich compartment devoid of antimicrobial
470 functions, and several intracellular bacteria derive their vacuole from, and/or
471 replicate in, this organelle [49]. Such is the case of *Legionella pneumophila* and
472 *Brucella abortus* that possess like *Wb* a type IV secretion system they employ
473 upon infection to secrete an array of effectors subverting cellular machineries to

474 gain access to ER. *L. pneumophila* regulate membrane trafficking through
475 modulations of GTPase signalling pathways interfering with early secretory
476 vesicles to ultimately allow fusion of the *Legionella* vacuole with ER-derived
477 membranes [50]. Along the endocytic pathway, *B. abortus* co-opt the ER exit sites
478 –ERES-, involved in the vesicular trafficking towards the Golgi., thus acquiring an
479 ER-derived vacuolar membrane [51]. Similar to observations of these pathogens,
480 our ultrastructural studies have revealed a tight association of *Wb* with rough ER
481 membranes. In addition, live experiments have demonstrated that some *Wb*-
482 containing vacuoles appear positive for a fluorescent and specific ER tracker, and
483 in some instances *Wb* were located within ER tubules, strongly suggesting that
484 the ER is a source of membrane for *Wb*. We hypothesize that the presence of ER
485 tracker-negative *Wb*-containing vacuoles indicates a maturation process in the
486 biogenesis of the membrane surrounding *Wb*, although we cannot rule out other
487 sources of membranes. The compaction of ER observed in both 1182-4 *Wb* and
488 S2R+ *Wb* cell lines places *Wb* in between ER and the Golgi apparatus, which
489 could potentially favors *Wb* interactions with the ERES. *Wb* could benefit from
490 co-opting the COPII vesicles routing towards the Golgi to acquire membranes,
491 lipids and other nutrients. This is in accordance with the discovery that in
492 presence of the pathogenic strain Wmelpop, cholesterol homeostasis is affected
493 [18]. Not only *Wb* likely incorporate cholesterol into their membranes as a
494 substitute for lipopolysaccharide, but also proper ER-to-Golgi vesicular
495 trafficking requires cholesterol [52]. Hence *Wb* may interfere with the
496 anterograde trafficking. In addition, a lipidomic analysis has shown that the
497 wMel affect the sphingolipid metabolism and deplete mosquito cells from
498 ceramide and derived sphingolipids [16]. Ceramides are synthesized in the ER

and exported to the Golgi [53]. They play an important role during bacterial infections as part of a pro-apoptotic lipid signalling [54] and sphingolipids regulate autophagosome biogenesis and endocytic trafficking [55], suggesting that a *Wb*-induced decreased availability of these lipids may prevent xenophagy and/or apoptosis. It is then possible that the interaction of *Wolbachia* with the ER and the derived intracellular vesicular trafficking plays also a central role in immune escape and control of apoptosis. In S2R+ *Wb* cells, the bacterial titer is exceptionally high compared to other infected insect cell lines, and *Wb* often fill the cytoplasm entirely when observed in confocal microscopy with an anti-WSP staining. In this cellular environment unable to efficiently control the *Wb* titer, electron microscopy analyses revealed a high frequency of poly *Wb*- containing vacuoles, possibly resulting from a limited access to new membranes. It is nonetheless interesting to observe that under these conditions the infection is persistent and does not compromise the host cell viability. Since ER tracker-negative *Wb* are often observed in the cell periphery, the interaction with ER may be necessary for an active replication.

Wb infections are usually characterized by very high intracellular loads of bacteria, usually above a hundred bacteria per cell, similar to other Rickettsiales. Despite the peculiar relationship between *Wb* and the ER, we did not detect an ER stress above levels found in non-infected cells suggesting that a *Wb* infection either does not require this cell response or is able to prevent it. Moreover, prolonged ER stress leads to cell death and seems incompatible with endosymbiosis [56,57]. This conclusion is in addition justified by several lines of evidence. First, although the ER appears redistributed, we did not detect morphological signs of enhanced ER activities linked to ER stress, such as

524 swollen tubules and cisternae, in contrast to a previous study performed with
525 wMel-infected LDW1 cells [19]. Second, we monitored the gene expression levels
526 for the three UPR sensors, downstream targets, and ERAD key players, either by
527 quantitative PCR or by fluorescent assay approaches. We could not find altered
528 gene expressions indicating that a persistent *Wb* infection triggers an ER stress.
529 Last, immunofluorescence studies of polyubiquitin linkages associated with
530 ERAD-driven proteolysis (K11 and K48 polyUb) revealed that these marks are
531 not increased in presence of *Wb.* Since the monoclonal antibody FK2 targets all
532 covalently linked mono- and poly-ubiquitins, it is likely that the increased
533 amount of FK2 foci in presence of *Wb* corresponds to either mono-ubiquitylated
534 proteins; and/or to proteins decorated with polyubiquitin chains on possibly the
535 five other lysine residues of ubiquitin with non-degradative roles, reported to be
536 involved in: K6 -mitophagy-, K27 -protein secretion and autophagy-, K63 -
537 endocytosis, signalling, activation of NF-kappa-B-; K33 -kinase modification-, and
538 K29 -lysosomal degradation- [38]. It is hence possible that *Wolbachia*, directly or
539 indirectly, influence a number of cellular mechanisms through modulation of
540 polyubiquitylation-dependent signalling events, and this field remains to be
541 explored. Recent proteomic studies provide conflictual evidence regarding *Wb*
542 and the UPR, possibly due to the differences in the *Wb* stains and the host cells
543 employed. The pathogenic strain wMelpop slightly increases (up to 1.36 fold)
544 some UPR–related genes identified by gene ontology analysis [18] while the wStr
545 infection in *Aedes albopictus* cells rather leads to a decrease of proteins involved
546 in ER protein folding [44]. Nonetheless a genome-wide RNAi screen has revealed
547 the importance of UBC6, an ubiquitin-conjugating enzyme part of the ERAD
548 pathway, to sustain the wMel titer [19]. Although we found no evidence for an

549 increased ERAD-induced proteolysis through ubiquitin-targeted proteasomal
550 degradation in presence of *Wb*, this does not rule out the requirement of intact
551 UPR/ERAD response for *Wb* survival. Alternatively, UBC6 may either be
552 involved in a non-ERAD-related function, or since the *Wb* vacuolar membrane
553 appears ER-derived, these endosymbionts may have subverted an ERAD
554 machinery at the level of their own vacuole. The apociplast of apicomplexan
555 parasites is an organelle derived from an algal endosymbiont that has retooled
556 the host ERAD into an apicoplast-localized ERAD-like protein import machinery
557 [58].
558 The UPR response can be modulated by intracellular pathogens to their
559 advantage, and the three branches –IRE1, PERK, ATF6- can be individually
560 upregulated or inhibited in order to modulate i.e. the host defense through
561 apoptosis or innate immunity response, or to build a replicative niche [59].
562 Hence, further investigations will be needed to clarify the role of the UPR in a
563 *Wb* infection. However, the absence of an enhanced ERAD-proteasomal
564 degradation pathway suggests that amino acid salvage does rely on mechanisms
565 other than an increased proteolysis. Several studies have shown that the *Wb*
566 infection decreases the global protein translation in the host cell [28,44]. While
567 the mechanisms are still unknown, TORC1 and insulin pathways regulate protein
568 translation based on environmental conditions, and greatly influence the *Wb*
569 titer in *Drosophila* [60]. Future studies will determine whether *Wolbachia* can
570 directly subvert growth signalling pathways to down-regulate translation and
571 therefore increase the pool of free amino acids.
572 In conclusion, there is no doubt that in an effort to elucidate the mechanisms of
573 intracellular survival employed by *Wolbachia*, the comprehension of subversion

574 strategies will be key: how are ubiquitylation pathways modulated and what are
575 their targets? How do *Wb* acquire ER-derived membranes on one hand, and how
576 do they modulate signalling or synthesis pathways to acquire amino acids and
577 lipids on the other hand? These are the next questions to be addressed. In
578 parallel, the current growing efforts to express the putative *Wb* effectors into
579 surrogate systems, yeast or *Drosophila* cell cultures, should accelerate our
580 knowledge of one of the most commonly encountered endosymbiont.
581
582
583

584 ## Methods

585 *Cell lines.*

586 All the cell lines are derived from primary cultures of *D. melanogaster* cells. JW18
587 is a kind gift from William Sullivan [61], 1182-4 was obtained from Alain Debec
588 [25,26], and S2R+ from François Juge [27]. JW18, 1182-4, and 1182-4*Wb* cells
589 were maintained in a Shields and Sang M3 insect medium (Sigma) supplemented
590 with 10% decomplemented fetal bovine serum and were passaged twice a week
591 at a 1/4 dilution. S2R+ and S2R+*Wb* cells were maintained in a Schneider insect
592 medium (Dominique Dutscher) supplemented with 10% decomplemented fetal
593 bovine serum and were passaged twice a week at a 1/2 dilution. Cell lines were
594 kept at 25°C.
595

596 *Extraction of Wolbachia from cell cultures.*

597 The content of ten 25 cm^2 cell culture flasks reaching confluency with *Wolbachia*-
598 infected JW18 adherent cells was pooled in two 50 mL Falcon tube and

599 centrifuged at 1200 rpm for 5 minutes at room temperature. Next, each pellet
600 was resuspended by pipetting on ice with 3 ml of pre-cooled Nalgene-filtered
601 extraction buffer (220 mM sucrose, 3.8 mM monopotassium phosphate, 8 mM
602 dipotassium phosphate, and 10 mM magnesium chloride).
603 Cell suspensions were transferred into two 15 ml Falcon conical tubes on ice
604 containing 2 g of sterile 3 mm-glass beads and vortexed vigorously 3 times for 30
605 seconds with a 30-second incubation period on ice between each round of
606 vortexing.
607 Each lysate was transferred to a new 15 ml Falcon tube on ice and centrifuged at
608 1200 rpm for 5 minutes at 4°C. Then, the *Wolbachia*-containing supernatant was
609 transferred to 1.5 mL Eppendorf tubes and centrifuged at 10 000 rpm for 10
610 minutes at 4°C to pellet *Wolbachia*.
611 The bacterial pellet of one of the Eppendorf tubes was resuspended in 500 µL of
612 cell culture medium and its content transferred from one tube to another in
613 order to resuspend all the bacterial pellets and collect them in one final tube.
614
615 *Generation of the Wolbachia-infected 1182-4Wb and S2R+Wb cell lines.*
616 An extract of *Wolbachia* was transferred into a 25 cm^2 cell culture flask
617 containing confluent 1182-4 or S2R+ cells in a 4 mL volume of cell culture
618 medium. After two days cells were passaged twice a week for a 1-month
619 duration and then, the infection process was repeated to obtain stably infected
620 1182-4*Wb* and S2R+*Wb* cell lines.
621 To follow the infection dynamics, cells were plated on 18 mm x 18 mm coverslips
622 in a plastic 6-well cell culture plate, and after adherence were fixed in PBS with
623 3.2% paraformaldehyde for 10 minutes at room temperature, washed for 5

minutes with PBS, and incubated for 2 hours at 37°C in the dark with Alexa Fluor 488 phalloidin A12379 (Life technologies) at a 1/50 dilution. After a 5-minute wash with PBS, coverslips were mounted on glass slides using Fluoroshield with DAPI and observed with an inverted laser scanning confocal microscope (SP5-SMD, Leica Microsystems) using a 63x/1.4 HCX PL APO CS oil objective and images taken with a z-stack interval of 0.5 µm.

The viability of 1182-4 versus 1182-4*Wb* and S2R+ versus S2R+*Wb* was evaluated using an automated cell counter (Countess Invitrogen) relying on a trypan blue (Life Technologies) exclusion method according to the protocol of the manufacturer. The cells were passaged the day before the viability measurements were taken.

Immunofluorescence studies.

Cells were plated on 18 mm x 18 mm coverslips in a 6-well cell culture plate 24 hours before fixation in PBS with 3.2% paraformaldehyde for 10 minutes at room temperature. Next, coverslips were dried and immersed in -20°C pre-cooled methanol and kept for 10 minutes at -20°C. Then, coverslips were dried out from residual methanol at room temperature and incubated in a humid chamber for 10 minutes with PBS, BSA 2%. After a PBS wash, cells were incubated for 2 hours at 37°C with the primary antibody or antibodies, added as a 50 µL drop. Following 3 washes of 5 minutes with PBS 1x, cells were incubated for 2 hours at 37°C with the secondary antibody or antibodies. Then, the cells were washed 3 times; each for 5 minutes with PBS 1x and mounted using fluoroshield with DAPI. All primary antibodies were used at a 1/400 dilution: rabbit polyclonal anti-GM130 antibody ab30637 (Abcam) and rabbit monoclonal

649 anti- K48 linkage polyubiquitin antibody ab140601 (Abcam). Mouse monoclonal
650 anti-FK2 ubiquitin antibody AB120 (LifeSensors). Rabbit monoclonal anti-
651 ubiquitin K11 linkage, clone 2A3/2E6 (Millipore). Mouse monoclonal anti-
652 *Wolbachia* surface protein (BEI resources, NIAID, NIH). Secondary antibodies
653 were used at a 1/500 dilution. Goat anti-mouse IgG antibody coupled to Alexa
654 Fluor 488 ab150117 (Abcam), goat anti-rabbit IgG antibody coupled to Cy3
655 A10520 (Invitrogen). An inverted laser scanning confocal microscope (SP5-SMD;
656 Leica Microsystems) at a scanning speed of 400 Hz equipped with a 63x/1.4 HCX
657 PL APO CS oil objective was used to take images with a z-stack= 0.5 µm and in
658 the case the images needed deconvolution (Deconvolution software: Huygens
659 Professional version 18.04), the z-stack= 0.2 µm.
660
661 *Drug treatments.*
662 Cells were incubated with tunicamycin (Sigma-Aldrich) at 10 µg/mL for 48 hours
663 [62].
664
665 *Live experiments.*
666 Cells were plated on concanavalin A-coated glass bottom fluorodishes 48 hours
667 before observation. One batch of the S2R+ cell line was treated with tunicamycin
668 as described above. To stain the ER, the cell culture medium was aspirated, cells
669 washed with PBS 1x and incubated for 30 minutes at 25°C with 1 µM live ER-
670 tracker red dye (Molecular Probes) diluted in PBS. The ER-tracker solution was
671 replaced by a 1/20 000 solution of SYTO-11 (Molecular Probes) DNA dye for 10
672 minutes at 25°C diluted in the appropriate cell culture medium prior to confocal
673 microscopy observations. The temperature of the microscope chamber was set

674 at 25°C prior to observation. For concomitant stainings of the ER and the Golgi
675 apparatus, cells were first incubated for 30 minutes at 4°C with 5 µM of BODIPY
676 FL C_5-ceramide (Molecular Probes) in PBS. Next, the cells were rinsed 3 times for
677 2 minutes and incubated for 30 minutes at 25°C with the live ER-tracker red dye
678 as described above. For SP5 confocal time-lapse recordings, stacks of three
679 images, z=0.5µm, were taken each 5 seconds, with a line average =8, in
680 bidirectional, resonance mode with a SP5 confocal microscope.
681 To monitor ATF4 activity, cells were plated on concanavalin A-coated glass
682 bottom fluorodishes. Upon cell adherence, the cells were transfected with a 4E-
683 BP intron-dsRed reporter plasmid [43] using the lipofectamine kit (Invitrogen)
684 according to the instructions of the manufacturer. Twenty-four hours post-
685 transfection, one of the fluorodishes containing *Wolbachia*-free cells was treated
686 with tunicamycin (10 µg/ml for 48 hours).
687
688
689 *Image analyses.*
690 The image analysis software used is ImageJ version 1.48. The ImageJ macros
691 were developed in collaboration with the MRI-CRBM-Optics plateform,
692 Montpellier, France and are available upon request. The graphing software used
693 was GraphPad Prism version 7.00.
694
695
696 *Electron microscopy.*
697 For each cell line, the content of a 25 cm^2 flask at cell confluence, three days after
698 medium change, was washed and transferred to a 1.5 mL Eppendorf tube and

699 centrifuged at 2000 rpm for 2 minutes at room temperature. The cell pellet was
700 fixed for 1 hour by resuspension in a 2.5% gluteraldehyde -PHEM solution
701 pH=7.4. Fixed cells were kept overnight at 4°C. Cells were next rinced in PHEM
702 buffer and post-fixed in 0.5% osmic acid for 2 hours at room temperature in the
703 dark. After two PHEM washes, cells were dehydrated in a graded series of
704 ethanol solutions (30-100%) before being embedded in EmBed 812 using an
705 automated microwave tissue processor for electron microscopy (Leica AMW).
706 Thin sections of 70 nm were collected at different levels of each block using the
707 Ultracut E microtome (Leica-Reichert). These sections were counterstained with
708 uranyl acetate and lead citrate and observed using a transmission electron
709 microscope (Tecnai F20) at 200 kV.
710
711 *RT-qPCR experiments.*
712 RNA extraction was performed in biological triplicates for each sample.
713 Precisely, the RNA was extracted from confluent flasks of 25 cm^2 containing
714 approximately 10^6 cells. The culture medium was aspirated and replaced by 1 ml
715 PBS 1x. Cells were scraped and transferred to 1.5 ml Eppendorf tubes and
716 centrifuged at 1200 rpm for 5 minutes. Following that, the supernatant was
717 discarded and the cells were resuspended in 300 µl of the Quick-RNA MicroPrep
718 kit (Zymo Research) lysis buffer. The next steps were performed according to the
719 RNA purification protocol detailed in the kits' instructions but the in-column
720 DNaseI treatment step was omitted and replaced with a TURBO DNase (Ambion)
721 treatment. RNA was purified using the RNA Clean & Concentrator-5 kit (Zymo
722 Research). cDNA was produced from 2 µg of RNA using the SuperScript VILO

cDNA synthesis kit (Invitrogen) and diluted at 1/25 for the RT-qPCR experiments.

Primer pairs were selected according to Primer3 version 0.4.0, synthesized by Eurofins Genomics (S1 table). Primer pairs with an efficiency close to 100% were selected for qPCR experiments.

RT-qPCR reactions were performed using SYBR Green 10x with Platinum Taq (Invitrogen). Amplifications were performed using a Mx3000P instrument (Agilent Technologies) and the MxPro QPCR Software (Agilent Technologies). The RT-qPCR cycling program consists of a pre-amplification cycle of 2 minutes at 94°C followed by 40 amplification cycles of 30 seconds at 94°C, 30 seconds at 55°C, and 20 seconds at 72°C. The RT-qPCR cycle ends with a dissociation/melt cycle of 1 minute at 94°C, 30 seconds at 55°C, and 30 seconds at 94°C.

For each gene, RT-qPCR is performed in technical and biological triplicates. The changes in expression were calculated according to the $2^{-\Delta\Delta Ct}$ method [63] and were plotted using the GraphPad Prism software version 7.0.

Acknowledgments

We thank Alain Debec for critical reading and providing the 1182-4 cell line, William Sullivan for providing the JW18 cell line, and the imaging facility MRI, member of the national infrastructure France-BioImaging supported by the French National Research Agency (ANR-10-INBS-04, «Investments for the future»), for developing macros for imaging quantification. The ATF4 activity reporter is a kind gift of Hyung Don Ryoo.

Figures

Figure 1

Influence of the genetic background of *Drosophila* cell lines on *Wolbachia* wMel titers.

(A) Summary of the experimental approach to infect 1182-4 and S2R+ cell lines. See Materials and Methods. (B to C') Confocal acquisitions of infected cell lines immunostained with an anti-WSP decorating the *Wolbachia* surface in cyan, DAPI is in magenta. (B') and (C') are higher magnifications showing individual cells corresponding to Supplemental movies 1 and 2. Scale bar= 10 microns. (D) Box plot graphs of *wMel* normalized titers in 1182-4 *Wb* and S2R+ *Wb*, expressed as a percentage of fluorescence surface associated with the anti-WSP staining per cell surface area (n= 181 and median= 11% for 1182-4 *Wb,* and n=215 and median= 71% for S2R+ *Wb*).

Figure 2

***Wolbachia* subcellular localization and titer do not influence the Golgi apparatus distribution and morphology.**

(A) Confocal acquisitions of infected cell lines immunostained with an anti- WSP -decorating the *Wolbachia* surface in cyan-, with GM130 -yellow-. DAPI is in magenta. Scale bars= 10 microns. Dashed lines encompass in S2R+ *Wb* a highly infected cell -left cell- and a infected cell at low level -right cell- (B) Top graphs: Distribution of GM-130 foci sizes in function of the *Wb* density measured on full projections of confocal images (n= 44 cells for 1182-4 *Wb* and n=46 cells for S2R+ *Wb*). Bottom graph: Amount of cis-Golgi expressed as GM130 total signal

772 per cell measured on full projections of confocal images, in infected and non-
773 infected cell lines (n= 1250 cells for 1182-4; 797 for 1182-4 *Wb*, and n=743 cells
774 for S2R+ cells and n=864 for S2R+ *Wb*). (C) Transmission electron microscopy
775 images of the Golgi apparatus in *Wolbachia*-infected cells. The Golgi stacks -
776 yellow arrows- appear normal (n>10, the red stars indicate the *trans*-Golgi).
777 Scale bars= 200 nm
778
779 **Figure 3**
780 ***Wolbachia* physically interact with the endoplasmic reticulum.**
781 (A) Time-lapse acquisitions at a surface focal plane in a 1182-4 *Wb* cell stained
782 with the DNA dye SYTO 11 -magenta- to highlight *Wb*, and an ER tracker -cyan-.
783 A t=0 second, grey arrows point to peripheral *Wb* clusters that are not in close
784 contact with the ER. The orange arrow points towards some *Wb* remaining in
785 close contact with the ER during the time lapse duration. The dotted yellow
786 circle highlights some *Wb* located within ER tubules. A single *Wb* within an ER
787 tubule is tracked by the plain yellow arrowhead, and its previous position is
788 indicated by an empty yellow arrowhead (i.e. at t=15s). Similarly, the movement
789 of a single *Wb* surrounded by an ER-derived membrane is tracked by green
790 arrowheads (t=15s to t=35s). See the corresponding supplemental movie 3. (B)
791 Scoring of *Wb*- ER interactions, observed with SYTO 11 and the ER tracker in
792 1182-*Wb* and S2R+ *Wb* cells, in random focal planes of n= 18 and n= 12 cells
793 respectively. Bacteria co-localized with ER tubules, or surrounded by an ER
794 tracker-positive membrane were counted as "ER-tracker positive". (C) The
795 different interactions between *Wb* and the ER are highlighted on these confocal
796 images, with clusters of *Wb* not in contact in 1182-4 *Wb* -see inset-. The

following rows are different examples in S2R+ cells showing i) *Wb* in close contact with the ER, ii) a *Wb* cluster composed of individual *Wb* surrounded with an ER tracker-positive membrane -yellow arrowheads-; iii) and in rare instances all individual *Wb* of the cell being surrounded with an ER tracker-positive membrane.

Figure 4

***Wolbachia* impact the ER distribution but not its structure in both S2R+ *Wb* and 1182-4 *Wb* cells.**

(A) Live imaging of S2R+ -top rows-, and S2R+ *Wb* -bottom rows- stained with SYTO 11 -magenta- and the ER tracker -cyan-. For S2R+ *Wb* cells, dashed lines encompass the nuclei, yellow arrowheads the colocalization of *Wb* and ER tubules, and blue arrows point to the clustered ER. The last row is a cortical focal plane showing the intense ER tubular network associated with *Wb*. Scale bar= 10µm. (B) Occurrence of clustered ER in various cell lines, with the addition of the S2R+ cell line treated with Tunicamycin at 10µg/mL for 48 hours. For S2R+ n= 179 ; S2R+ *Wb* n= 123; S2R+ with Tunicamycin n=227; 1182-4 n=76; 1182-4 *Wb* n=120. (C) Electron micrograph of S2R+ and S2R+ *Wb*. The top row highlights the presence of a darker ER mass -red arrow-, numerous *Wb* are visible in between the nucleus and the ER cluster. The second row is a series of consecutive enlargements of an ER cluster in the vicinity of vacuoles containing multiple *Wb* -orange arrowheads pointing to the vacuolar membrane-. Green arrows and the red arrow indicate the tubular ER and piled ER membranes respectively. Cyan arrows point towards ER membranes encompassing vacuoles containing multiple *Wb* in the cell periphery. The last image depicts a single

822 vacuole with multiple *Wb*, tightly surrounded by rough ER -cyan arrow-. Scale
823 bar= 500 nm. (D) The ER inter-membrane distance in the different cell lines.
824 Measurements were taken on high magnification electron micrographs as
825 depicted -red line-, and the average thickness varies from 42 to 56 nm. For S2R+
826 n=75 ; S2R+ *Wb* n=43; 1182-4 n=35; 1182-4 *Wb* n=58. (E) Live imaging of S2R+
827 and S2R+ *Wb* cells stained simultaneously with ER -cyan- and Golgi -red-
828 fluorescent trackers. Upper panels are lower magnifications and lower panels
829 are higher magnifications. Arrowheads point towards Golgi foci. Scale bar=10µm.
830
831 **Figure 5**
832 **Polyubiquitin linkages associated with ERAD and proteosomal degradation**
833 **are not increased in presence of *Wolbachia*.**
834 (A) Confocal acquisitions of the infected and non-infected 1182-4 and S2R+ cell
835 lines stained with DAPI -magenta- and the monoclonal antibody FK2 -yellow-,
836 recognizing all mono- and poly-ubiquitylated proteins, but not free ubiquitin.
837 Dashed lines encompass individual cells, scale bar=10 µm. (B) Box plot graphs
838 showing the FK2-positive foci quantification, expressed as total areas per full
839 confocal projections in individual cells. For 1182-4 n=218; 1182-4 *Wb* n=106;
840 S2R+ n= 212; S2R+ *Wb* n= 195 cells. (C) Linear regression of the FK2-positive
841 total area per 1182-*Wb* cell, in function of the *Wb* titer, established on the DAPI
842 signal (cf. Materials and Methods), n=104 cells. (D) Confocal acquisitions of the
843 infected and non-infected 1182-4 and S2R+ cell lines stained with WSP -
844 magenta- and an anti- K11-linkage polyubiquitin -yellow-. The dashed line
845 highlights the cell area of a heavily *Wb*-infected S2R+ *Wb* cell, containing a mass
846 of ER, physically excluding the endosymbionts. Scale bar= 10µm.

847

848 **Figure 6**

849 ***Wolbachia* do not induce induce ER stress.**

850 (A) Schematic summary of the UPR and ERAD pathways. The color code
851 highlights the three UPR pathways and the ERAD and is identical to what
852 employed in (B). (B) Genes tested by quantitative PCR, in presence of
853 tunicamycin -top graphs-, or Wolbachia -bottom graphs-. UPR genes are on the
854 left and ERAD genes on the right. Gene expression fold changes are represented,
855 and variations comprised between a 2-fold increased expression -"2" above the
856 dashed line- and a 2-fold decreased expression - "0.5" are considered
857 insignificant. (C) S2R+ cells transfected with the ATF4 activity reporter E-BP
858 intron dsRed; after a 48hr-long treatment with tunicamycin at 10 µg/mL, or in
859 presence of *Wb*. DNA is stained with SYTO-11 -green-. In absence of *Wb*, nuclei
860 incorporate the dye at various levels, while in presence of *Wb*, the dye stains
861 preferentially the endosymbionts compared to the nuclei, highlighted with a red
862 dashed line. Two adjacent transfected cells are shown in presence of
863 tunicamycin, and only one for S2R+ and S2R+ *Wb*. The graph represents
864 quantifications of the dsRed fluorescence levels in each conditions. For S2R+
865 n=14; S2R+ with tunicamycin n=11; and for S2R+ *Wb* n=15.

866

867

868 ## Supporting information

869

870 **S1 Fig. Infection of naive cell lines**

(A) Infection dynamics of 1182-4 cells challenged with purified wMel *Wolbachia.* Scoring of intracellular *Wb* was performed on confocal images of fixed cells at the various time points represented on the graph, with a phalloidin staining -yellow- to visualize the cortical actin in order to count the number of intracellular *Wb* only, per individual cells. *Wb* are detected as DAPI bright cytoplasmic foci(- magenta-, i.e. green arrow pointing at a single bacterium at an early time point). Scale bar= 10 µm, n=100 cells per time point, counted in randomly acquired images per coverslip. (B) Cell survival established with Trypan blue. Analyses were performed 24 hr-post medium change.

S2 Fig. Anti- K48-linkage polyubiquitin immunostainings.

Confocal acquisitions of the infected and non-infected 1182-4 and S2R+ cell lines stained with WSP -magenta- and an anti- K48-linkage polyubiquitin -yellow-.

S1 Movie. A *Wolbachia*-infected 1182-4 cell.

A 1182-4 cell infected by JW18-derived wMel. This animation shows the different Z stacks composing the corresponding confocal merged image in Fig.1. WSP decorates the *Wolbachia* in Cyan and DAPI is in magenta.

S2 Movie. A *Wolbachia*-infected S2R+ cell.

A S2R+ cell infected by JW18-derived *wMel*. This animation shows the different Z stacks composing the corresponding confocal merged image in Fig.1. WSP decorates the *Wolbachia* in Cyan and DAPI is in magenta.

S3 Movie. Time lapse recording of *Wolbachia* and the ER in a 1182-4*Wb* cell.

Time lapse acquisitions of a surface focal place in an 1182-4 *Wb* cell. Images are taken each 5 seconds, and the cell is stained with the live DNA dye SYTO 11 to track the *Wolbachia* -magenta- and the ER-tracker is in cyan.

S1 Table. List of selected primers for qPCR analyses.

References

1. Werren JH, Baldo L, Clark ME. Wolbachia: master manipulators of invertebrate biology. Nat Rev Microbiol. 2008;6: 741–751. doi:10.1038/nrmicro1969
2. Pietri JE, DeBruhl H, Sullivan W. The rich somatic life of Wolbachia. Microbiologyopen. 2016;5: 923–936. doi:10.1002/mbo3.390
3. Unckless RL, Boelio LM, Herren JK, Jaenike J. Wolbachia as populations within individual insects: Causes and consequences of density variation in natural populations. Proc R Soc B Biol Sci. 2009;276: 2805–2811. doi:10.1098/rspb.2009.0287
4. Toomey ME, Panaram K, Fast EM, Beatty C, Frydman HM. Evolutionarily conserved Wolbachia-encoded factors control pattern of stem-cell niche tropism in Drosophila ovaries and favor infection. Proc Natl Acad Sci U S A. 2013;110: 10788–93. doi:10.1073/pnas.1301524110
5. Chrostek E, Teixeira L. Mutualism Breakdown by Amplification of

921 Wolbachia Genes. PLoS Biol. 2015;13: 1–22.
922 doi:10.1371/journal.pbio.1002065
923 6. Serbus LR, Sullivan W. A cellular basis for Wolbachia recruitment to the
924 host germline. PLoS Pathog. 2007;3: 1930–1937.
925 doi:10.1371/journal.ppat.0030190
926 7. Slatko BE, Taylor MJ, Foster JM. The Wolbachia endosymbiont as an anti-
927 filarial nematode target. Symbiosis. 2010;51: 55–65. doi:10.1007/s13199-
928 010-0067-1
929 8. Jiggins FM. The spread of Wolbachia through mosquito populations. PLoS
930 Biol. 2017;15: 1–6. doi:10.1371/journal.pbio.2002780
931 9. Teixeira L, Ferreira Á, Ashburner M. The Bacterial Symbiont Wolbachia
932 Induces Resistance to RNA Viral Infections in Drosophila melanogaster.
933 Keller L, editor. PLoS Biol. 2008;6: e1000002.
934 doi:10.1371/journal.pbio.1000002
935 10. M. L, Hedges, Jeremy C. Brownlie, Scott L. O'Neill KNJ. Wolbachia and Virus
936 Protection in Insects. Science (80-). 2008;322: 702.
937 11. Lindsey ARI, Bhattacharya T, Newton ILG, Hardy RW. Conflict in the
938 intracellular lives of endosymbionts and viruses: A mechanistic look at
939 Wolbachia-mediated pathogen-blocking. Viruses. 2018;10: 1–29.
940 doi:10.3390/v10040141
941 12. Rancès E, Ye YH, Woolfit M, McGraw EA, O'Neill SL. The relative
942 importance of innate immune priming in Wolbachia-mediated dengue
943 interference. PLoS Pathog. 2012;8. doi:10.1371/journal.ppat.1002548
944 13. Molloy J, Sinkins S. Wolbachia Do Not Induce Reactive Oxygen Species-
945 Dependent Immune Pathway Activation in Aedes albopictus. Viruses.

2015;7: 4624–4639. doi:10.3390/v7082836

14. Foster J, Ganatra M, Kamal I, Ware J, Makarova K, Ivanova N, et al. The Wolbachia Genome of Brugia malayi: Endosymbiont Evolution within a Human Pathogenic Nematode. PLoS Biol. 2005;3: e121. doi:10.1371/journal.pbio.0030121

15. Wu M, Sun L V., Vamathevan J, Riegler M, Deboy R, Brownlie JC, et al. Phylogenomics of the reproductive parasite Wolbachia pipientis wMel: A streamlined genome overrun by mobile genetic elements. PLoS Biol. 2004;2: 327–341. doi:10.1371/journal.pbio.0020069

16. Molloy JC, Sommer U, Viant MR, Sinkins SP. Wolbachia Modulates Lipid Metabolism in Aedes albopictus Mosquito. 2016;82: 3109–3120. doi:10.1128/AEM.00275-16.Editor

17. Caragata EP, Rancès E, Hedges LM, Gofton AW, Johnson KN, O'Neill SL, et al. Dietary Cholesterol Modulates Pathogen Blocking by Wolbachia. PLoS Pathog. 2013;9. doi:10.1371/journal.ppat.1003459

18. Geoghegan V, Stainton K, Rainey SM, Ant TH, Dowle AA, Larson T, et al. Perturbed cholesterol and vesicular trafficking associated with dengue blocking in Wolbachia-infected Aedes aegypti cells. Nat Commun. Springer US; 2017;8: 526. doi:10.1038/s41467-017-00610-8

19. White PM, Serbus LR, Debec A, Codina A, Bray W, Guichet A, et al. Reliance of wolbachia on high rates of host proteolysis revealed by a genome-wide RNAi screen of Drosophila cells. Genetics. 2017;205: 1473–1488. doi:10.1534/genetics.116.198903

20. Schwarz DS, Blower MD. The endoplasmic reticulum: Structure, function and response to cellular signaling. Cell Mol Life Sci. Springer Basel;

971 2016;73: 79–94. doi:10.1007/s00018-015-2052-6

972 21. Romero-Brey I, Bartenschlager R. Endoplasmic reticulum: The favorite
973 intracellular niche for viral replication and assembly. Viruses. 2016;8: 1–
974 26. doi:10.3390/v8060160

975 22. Celli J, Tsolis RM. Bacteria , the ER and the Unfolded Protein Response :
976 Friends or. Nat Rev Microbiol. 2015;13: 71–82.
977 doi:10.1038/nrmicro3393.Bacteria

978 23. Sano R, Reed JC. ER stress-induced cell death mechanisms. Biochim
979 Biophys Acta - Mol Cell Res. Elsevier B.V.; 2013;1833: 3460–3470.
980 doi:10.1016/j.bbamcr.2013.06.028

981 24. Cherbas L, Willingham A, Zhang D, Yang L, Zou Y, Eads BD, et al. The
982 transcriptional diversity of 25 Drosophila cell lines. Genome Res. 2011;21:
983 301–314. doi:10.1101/gr.112961.110

984 25. Debec A. Haploid cell cultures of Drosophila melanogaster. Nature. 1978.
985 pp. 255–256. doi:10.1038/274255a0

986 26. Debec A, Abbadie C. The acentriolar state of the Drosophila cell lines 1182.
987 Biol Cell. 1989;67: 307–311. doi:10.1111/j.1768-322X.1989.tb00876.x

988 27. Yanagawa S, Lee J, Ishimoto A, Chem JB. Identification and
989 Characterization of a Novel Line of Drosophila Schneider S2 Cells That
990 Respond to Wingless Signaling Identification and Characterization of a
991 Novel Line of Drosophila Schneider S2 Cells That Respond to Wingless
992 Signaling *. Jounral Biol Chem. 1998;273: 32353–32359.

993 28. Grobler Y, Yun CY, Kahler DJ, Bergman CM, Lee H, Oliver B, et al. Whole
994 genome screen reveals a novel relationship between Wolbachia levels and
995 Drosophila host translation. bioRxiv. 2018; doi:10.1101/380485

29. Bhattacharya T, Newton ILG, Hardy RW. Wolbachia elevates host methyltransferase expression to block an RNA virus early during infection. PLoS Pathog. 2017;13: 1–22. doi:10.1371/journal.ppat.1006427

30. White PM, Pietri JE, Debec A, Russell S, Patel B, Sullivan W. Mechanisms of Horizontal Cell-to-Cell Transfer of Wolbachia spp. in Drosophila melanogaster. Drake HL, editor. Appl Environ Microbiol. 2017;83: e03425-16. doi:10.1128/AEM.03425-16

31. Rainey SM, Martinez J, McFarlane M, Juneja P, Sarkies P, Lulla A, et al. Wolbachia Blocks Viral Genome Replication Early in Infection without a Transcriptional Response by the Endosymbiont or Host Small RNA Pathways. PLoS Pathog. 2016;12: 1–22. doi:10.1371/journal.ppat.1005536

32. van Bergeijk P, Hoogenraad CC, Kapitein LC. Right Time, Right Place: Probing the Functions of Organelle Positioning. Trends Cell Biol. Elsevier Ltd; 2016;26: 121–134. doi:10.1016/j.tcb.2015.10.001

33. Romano JD, Coppens I. Host Organelle Hijackers: A similar modus operandi for Toxoplasma gondii and Chlamydia trachomatis: Co-infection model as a tool to investigate pathogenesis. Pathog Dis. 2013;69: 72–86. doi:10.1111/2049-632X.12057

34. Cho KO, Kim GW, Lee OK. Wolbachia bacteria reside in host Golgi-related vesicles whose position is regulated by polarity proteins. PLoS One. 2011;6. doi:10.1371/journal.pone.0022703

35. Heuer D, Lipinski AR, Machuy N, Karlas A, Wehrens A, Siedler F, et al. Chlamydia causes fragmentation of the Golgi compartment to ensure reproduction. Nature. Nature Publishing Group; 2009;457: 731–735.

1021 doi:10.1038/nature07578

1022 36. Casper-Lindley C, Kimura S, Saxton DS, Essaw Y, Simpson I, Tan V, et al.
1023 Rapid Fluorescence-Based Screening for Wolbachia Endosymbionts in
1024 Drosophila Germ Line and Somatic Tissues. Appl Environ Microbiol.
1025 2011;77: 4788–4794. doi:10.1128/AEM.00215-11

1026 37. Hwang J, Qi L. Quality Control in the Endoplasmic Reticulum: Crosstalk
1027 between ERAD and UPR pathways. Trends Biochem Sci. Elsevier Ltd;
1028 2018;43: 593–605. doi:10.1016/J.TIBS.2018.06.005

1029 38. Swatek KN, Komander D. Ubiquitin modifications. Cell Res. Nature
1030 Publishing Group; 2016;26: 399–422. doi:10.1038/cr.2016.39

1031 39. Xu P, Duong DM, Seyfried NT, Cheng D, Xie Y, Rush J, et al. Quantitative
1032 Proteomics Reveals the Function of Unconventional Ubiquitin Chains in
1033 Proteasomal Degradation. 2009;137: 133–145.
1034 doi:10.1016/j.cell.2009.01.041.Quantitative

1035 40. Locke M, Toth J, Petroski M. K11- and K48-Linked Ubiquitin Chains
1036 Interact with p97 during Endoplasmic Reticulum-Associated Degradation.
1037 Biochem J. 2014;459: 205–216.
1038 doi:10.1016/j.pestbp.2011.02.012.Investigations

1039 41. Bravo R, Parra V, Gatica D, Rodriguez AE, Torrealba N, Paredes F, et al.
1040 Endoplasmic Reticulum and the Unfolded Protein Response. Scientifica.
1041 2013. pp. 215–290. doi:10.1016/B978-0-12-407704-1.00005-1

1042 42. Chow CY, Wolfner MF, Clark AG. Using natural variation in Drosophila to
1043 discover previously unknown endoplasmic reticulum stress genes. Proc
1044 Natl Acad Sci. 2013;110: 9013–9018. doi:10.1073/pnas.1307125110

1045 43. Kang MJ, Vasudevan D, Kang K, Kim K, Park JE, Zhang N, et al. 4E-BP is a

target of the GCN2 – ATF4 pathway during Drosophila development and aging. J Cell Biol. 2016;216: 1–15. doi:10.1083/jcb.201511073

44. Baldridge G, Higgins L, Witthuhn B, Markowski T, Armien A, Fallon A, et al. Proteomic analysis of a mosquito host cell response to persistent Wolbachia infection. Res Microbiol. 2017;168: 609–625. doi:10.1016/j.resmic.2017.04.005.For

45. Fallon AM, Witthuhn BA. Proteasome activity in a naïve mosquito cell line infected with Wolbachia pipientis wAlbB. Vitr Cell Dev Biol - Anim. 2009;45: 460–466. doi:10.1007/s11626-009-9193-6

46. Frydman HM, Li JM, Robson DN, Wieschaus E. Somatic stem cell niche tropism in Wolbachia. Nature. 2006;441: 509–512. doi:10.1038/nature04756

47. Landmann F, Bain O, Martin C, Uni S, Taylor MJ, Sullivan W. Both asymmetric mitotic segregation and cell-to-cell invasion are required for stable germline transmission of Wolbachia in filarial nematodes. Biol Open. 2012;1: 536–547. doi:10.1242/bio.2012737

48. Fenollar F, Maurin M, Raoult D. Wolbachia pipientis growth kinetics and susceptibilities to 13 antibiotics determined by immunofluorescence staining and real-time PCR. Antimicrob Agents Chemother. 2003;47: 1665–1671. doi:10.1128/AAC.47.5.1665-1671.2003

49. Celli J, Tsolis RM. Bacteria , the ER and the Unfolded Protein Response : Friends or. 2016;13: 71–82. doi:10.1038/nrmicro3393.Bacteria

50. Santos JC, Enninga J. At the crossroads: communication of bacteria-containing vacuoles with host organelles. Cell Microbiol. 2016;18: 330–339. doi:10.1111/cmi.12567

1071 51. Celli J. The changing nature of the Brucella-containing vacuole. Cell
1072 Microbiol. 2015;17: 951–958. doi:10.1111/cmi.12452
1073 52. Ridsdale A. Cholesterol Is Required for Efficient Endoplasmic Reticulum-
1074 to-Golgi Transport of Secretory Membrane Proteins. Mol Biol Cell.
1075 2006;17: 1593–1605. doi:10.1091/mbc.E05-02-0100
1076 53. Hanada K. Ceramide Transport from the Endoplasmic Reticulum to the
1077 Trans Golgi Region at Organelle Membrane Contact Sites. 2017. pp. 69–81.
1078 doi:10.1007/978-981-10-4567-7_5
1079 54. Mullen TD, Obeid LM. Ceramide and Apoptosis: Exploring the Enigmatic
1080 Connections between Sphingolipid Metabolism and Programmed Cell
1081 Death. Anticancer Agents Med Chem. 2012;12: 340–363.
1082 doi:10.2174/187152012800228661
1083 55. Young MM, Wang H-G. Sphingolipids as Regulators of Autophagy and
1084 Endocytic Trafficking. Advances in Cancer Research. 2018. pp. 27–60.
1085 doi:10.1016/bs.acr.2018.04.008
1086 56. Logue SE, Cleary P, Saveljeva S, Samali A. New directions in ER stress-
1087 induced cell death. Apoptosis. 2013;18: 537–546. doi:10.1007/s10495-
1088 013-0818-6
1089 57. Shore GC, Papa FR, Oakes SA. Signaling cell death from the endoplasmic
1090 reticulum stress response. Curr Opin Cell Biol. 2011;23: 143–149.
1091 doi:10.1016/j.ceb.2010.11.003
1092 58. Agrawal S, Chung DWD, Ponts N, van Dooren GG, Prudhomme J, Brooks CF,
1093 et al. An Apicoplast Localized Ubiquitylation System Is Required for the
1094 Import of Nuclear-encoded Plastid Proteins. PLoS Pathog. 2013;9.
1095 doi:10.1371/journal.ppat.1003426

59. Cornejo E, Schlaermann P, Mukherjee S. How to rewire the host cell: A home improvement guide for intracellular bacteria. J Cell Biol. 2017;216: 3931–3948. doi:10.1083/jcb.201701095

60. Serbus LR, White PM, Silva JP, Rabe A, Teixeira L, Albertson R, et al. The Impact of Host Diet on Wolbachia Titer in Drosophila. PLoS Pathog. 2015;11: 1–25. doi:10.1371/journal.ppat.1004777

61. Serbus LR, Landmann F, Bray WM, White PM, Ruybal J, Lokey RS, et al. A Cell-Based Screen Reveals that the Albendazole Metabolite, Albendazole Sulfone, Targets Wolbachia. PLoS Pathog. 2012;8.

62. Plongthongkum N, Kullawong N, Panyim S, Tirasophon W. Ire1 regulated XBP1 mRNA splicing is essential for the unfolded protein response (UPR) in Drosophila melanogaster. Biochem Biophys Res Commun. 2007;354: 789–794. doi:10.1016/j.bbrc.2007.01.056

63. Livak KJ, Schmittgen TD. Analysis of relative gene expression data using real-time quantitative PCR and the 2-ΔΔCT method. Methods. 2001;25: 402–408. doi:10.1006/meth.2001.1262

1121

1122

1123

1124

1125

1126

1127

1128

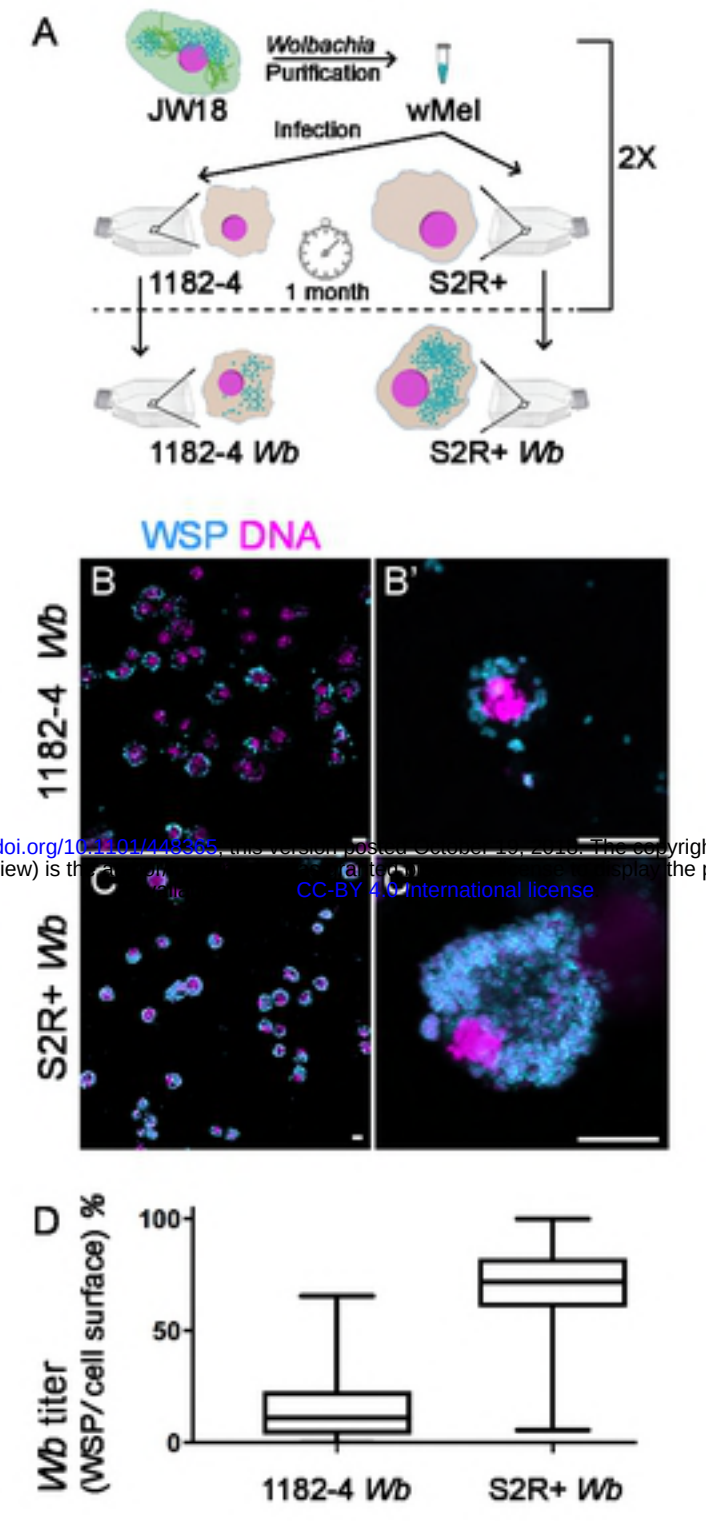

Figure 1

Fig1

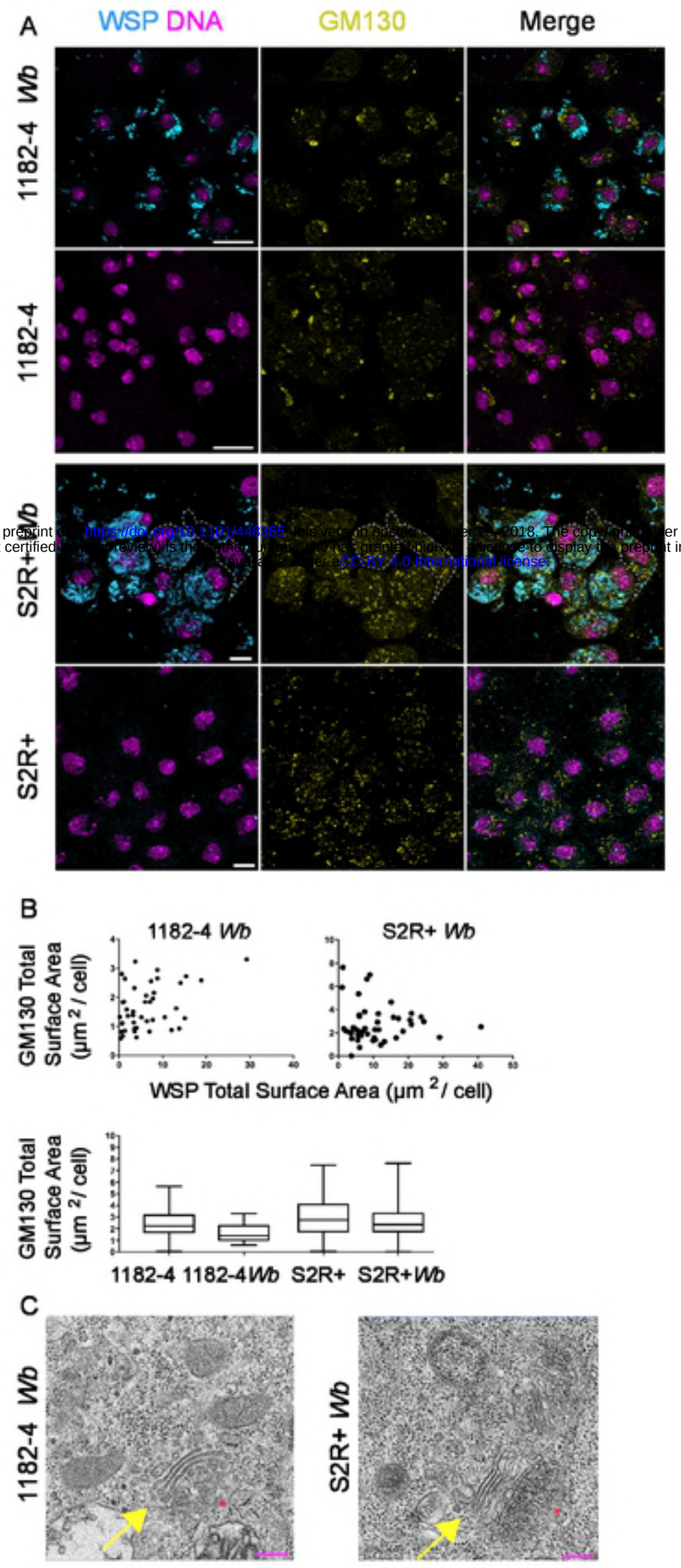

Figure 2

Fig2

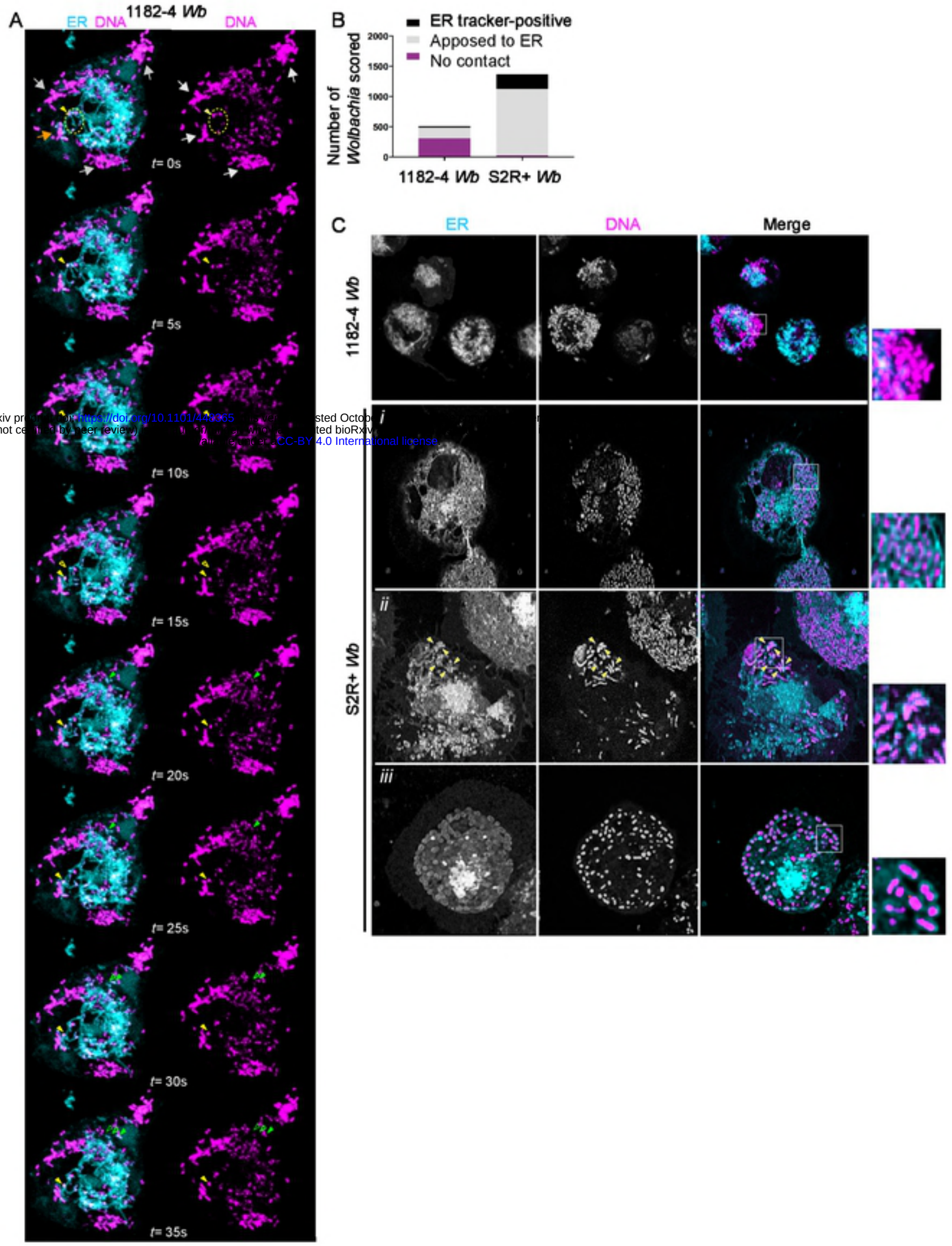

Figure 3

Fig3

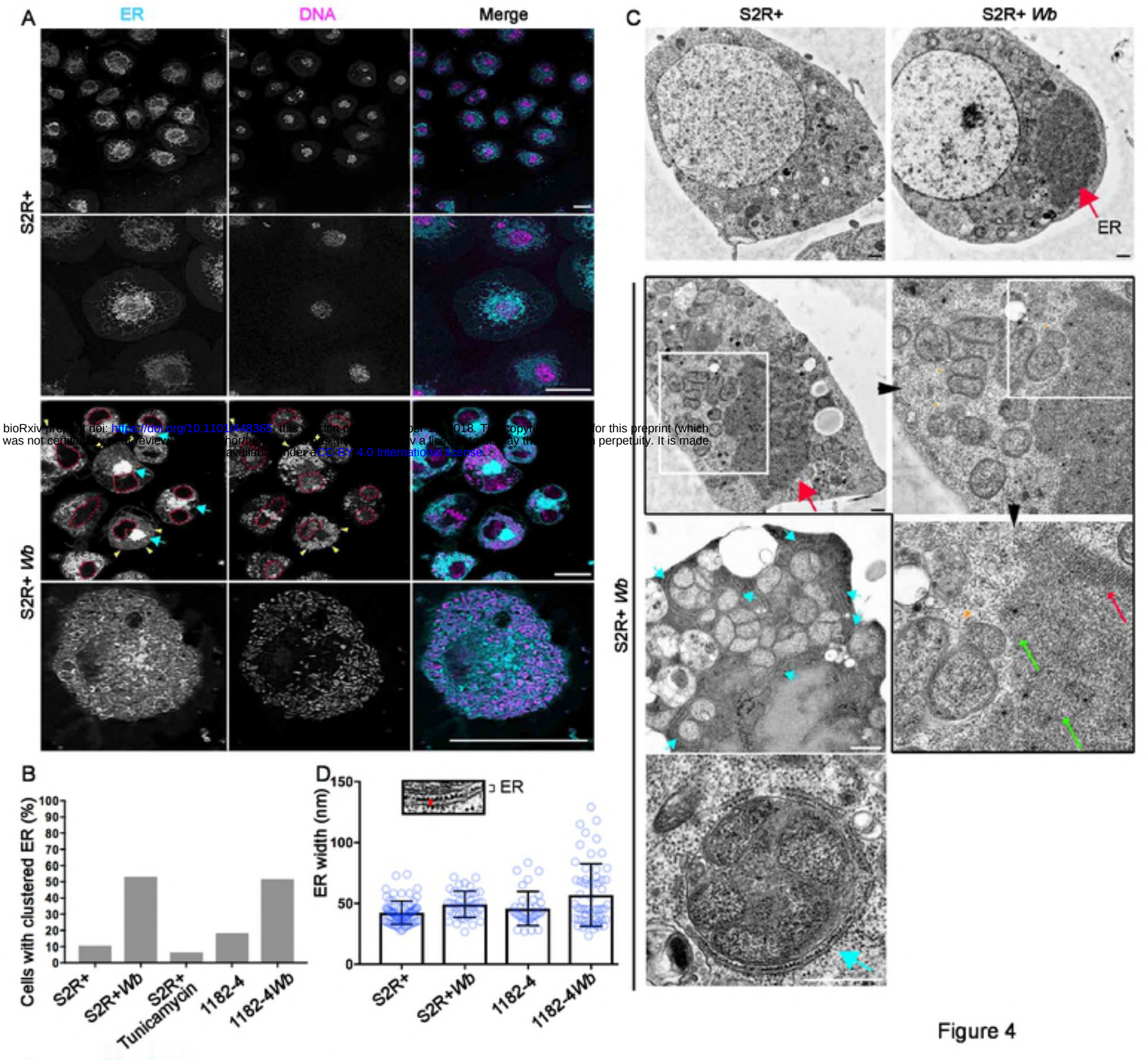

Figure 4

Fig4

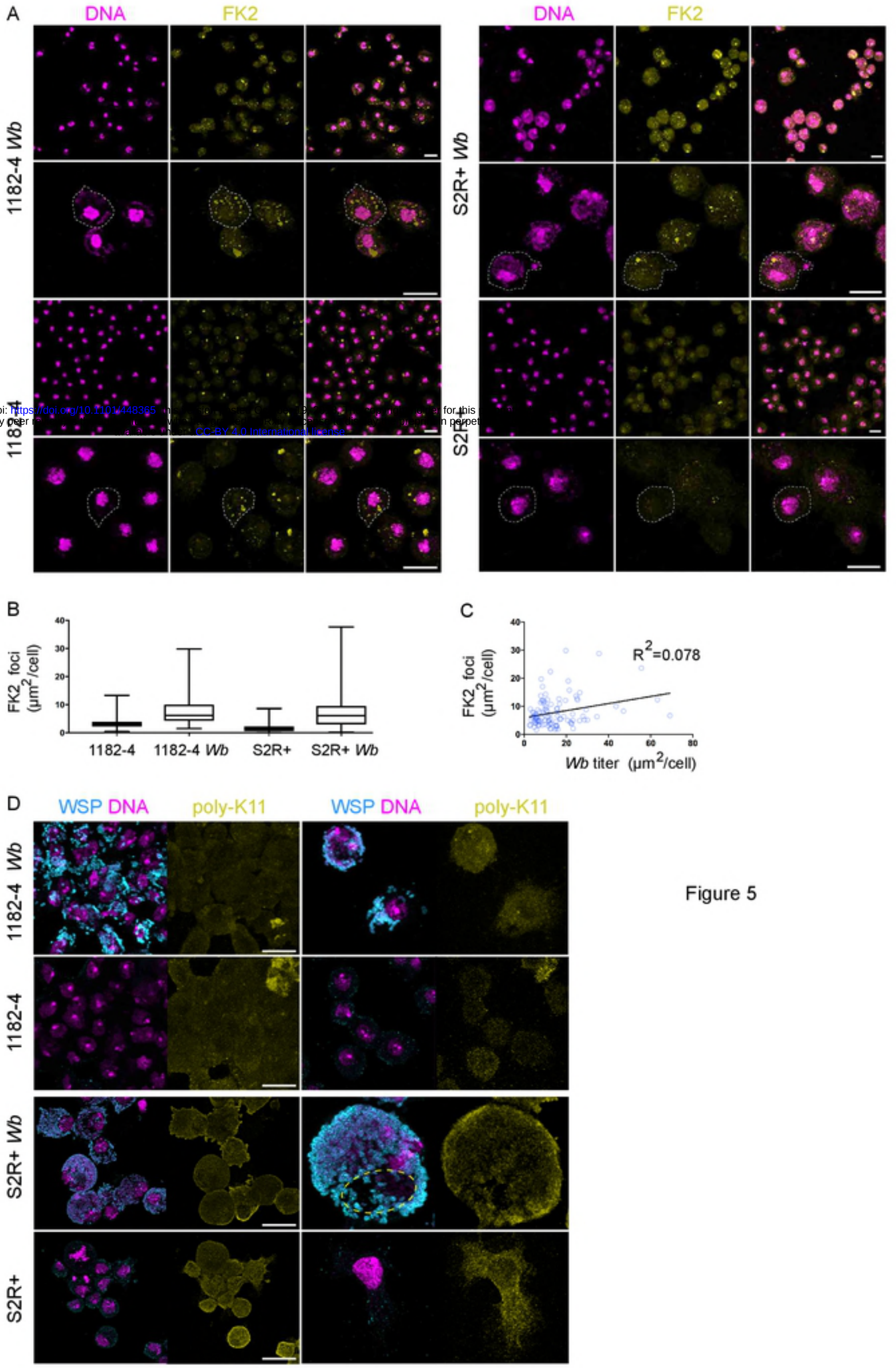

Figure 5

Fig5

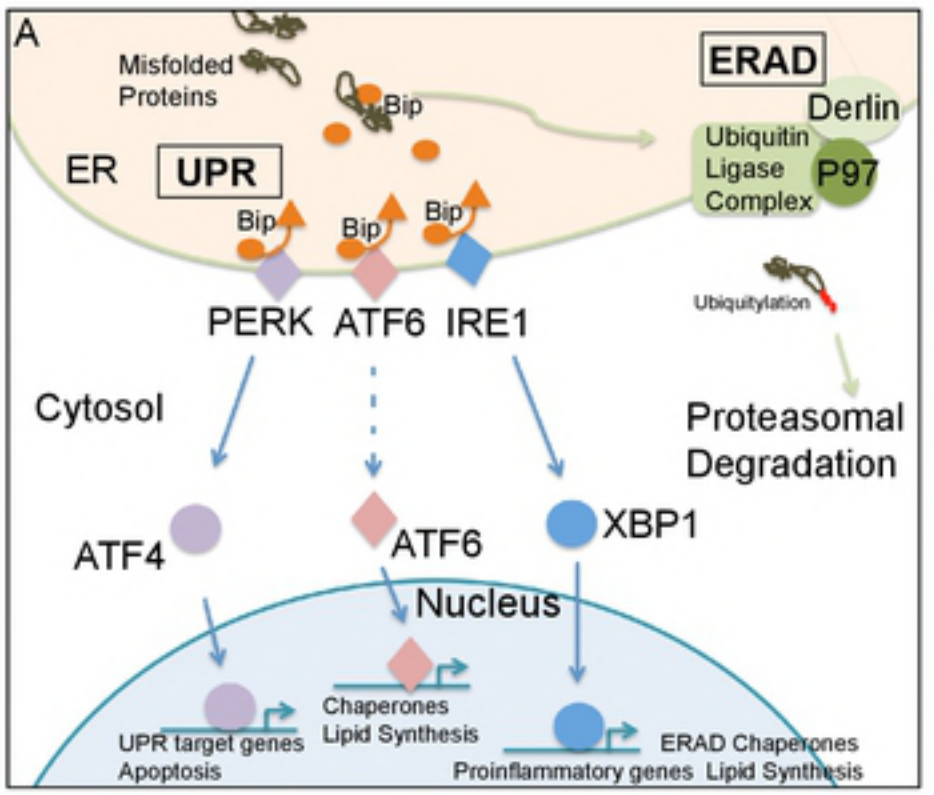

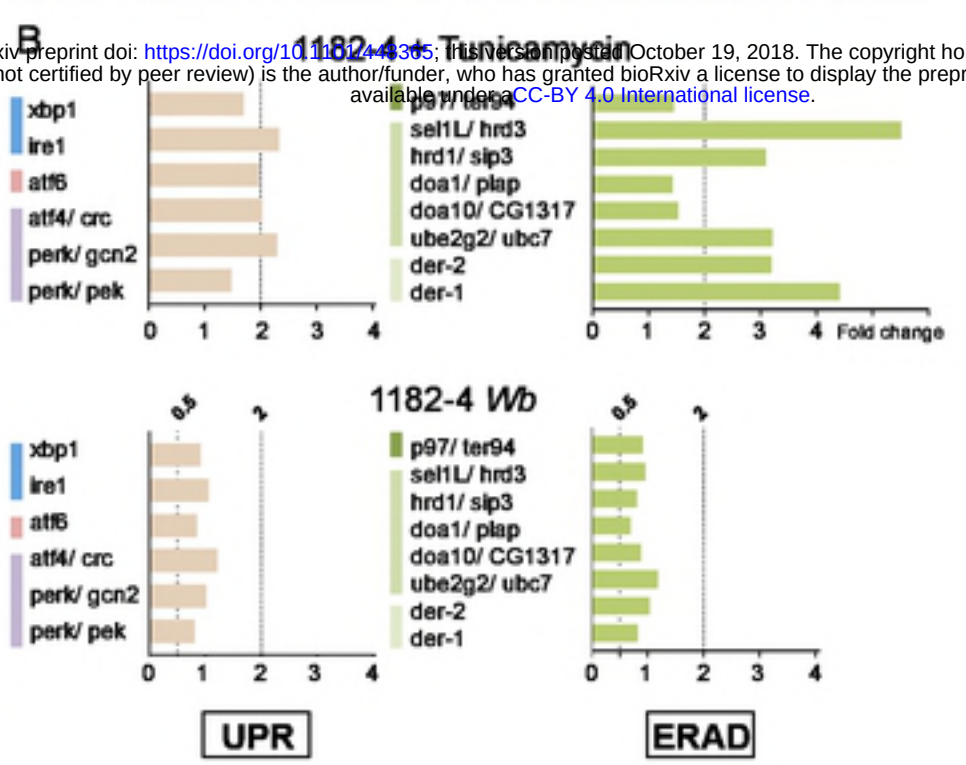

Figure 6

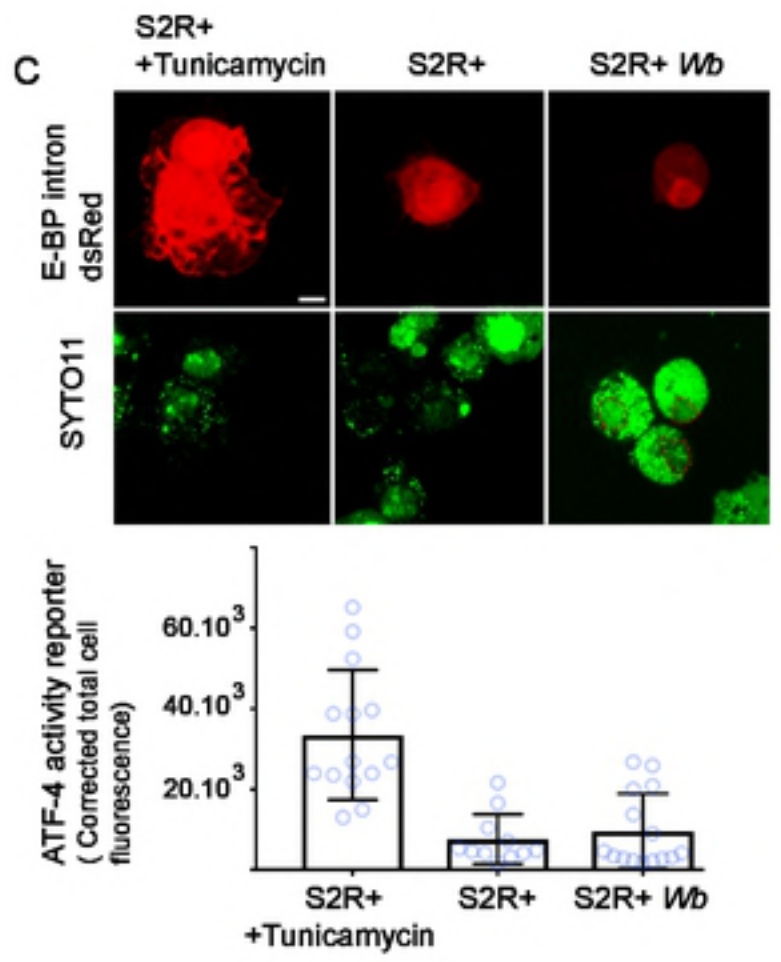

Fig6